

Anisotropic Diffusion Modeling of Cosmic-Ray Lepton Propagation

V.D. Borisov ^{1,2,*} and I.A. Kudryashov ^{2,†}

¹*Faculty of Physics, M.V. Lomonosov Moscow State University (MSU), 119991 Moscow, Russia*

²*Skobeltsyn Institute of Nuclear Physics, Lomonosov Moscow State University (MSU), 119991 Moscow, Russia*

(Dated: December 9, 2025)

Abstract

We analyze DAMPE and H.E.S.S. measurements of the total cosmic-ray electron-positron spectrum, together with the AMS-02 positron fraction, using an anisotropic, spatially varying diffusion framework. The diffusion-tensor components are computed via numerical integration of test-particle trajectories in a prescribed Galactic magnetic-field model. We show that accounting simultaneously for the spatial dependence and anisotropy of the diffusion tensor yields an accurate description of the local electron and positron data up to TeV energies. The inferred injection spectral index, $\Gamma = -2.169$, is fully consistent with expectations from diffusive shock-acceleration theory. Within this framework, the observed spectral softening arises naturally from enhanced energy losses experienced by leptons propagating over larger distances along the regular magnetic field.

I. INTRODUCTION

A detailed understanding of cosmic-ray (CR) propagation in the Galactic magnetic field is essential for establishing a consistent connection between the physical processes operating in the interstellar medium and a wide range of observables, including local particle spectra as well as diffuse γ -ray

and radio emission. The reliability of such a connection depends both on the realism of the adopted Galactic geometry and source, gas, and radiation-field distributions, and on the choice of the transport framework.

Existing approaches span a wide range of complexity. Analytic Green's-function solutions [1], applicable to homogeneous or symmetric media, offer convenient estimates and enable controlled studies of individual sources. However, they require diffusion pa-

* sw.vladislav.b@gmail.com

† ilya.kudryashov.85@gmail.com

rameters borrowed from more complete numerical models and lose applicability when describing global diffuse emission; see, e.g., [2] for a review. More advanced diffusion and stochastic codes—such as GALPROP [3], DRAGON2 [4], and CRPropa [5]—solve the CR transport equation within a three-dimensional Galactic structure and reproduce a broad range of observational data. Nevertheless, the diffusion approximation itself relies on several nontrivial assumptions: a clear separation of scales between the Larmor radius and large-scale magnetic-field gradients, quasi-linear interactions with turbulence, and approximate statistical homogeneity on diffusion scales. These assumptions may break down near sources [6], in shock environments, in regions of strong magnetic-field anisotropy, and in the transition between ballistic and diffusive regimes; see, e.g., [7] for details. In contrast, direct numerical methods—such as test-particle trajectory integration in prescribed 3D magnetic fields or fully self-consistent MHD simulations—circumvent the diffusion approximation and explicitly track particle dynamics. However, the computational cost increases sharply toward lower energies because of the decreasing Larmor radius and the need to resolve an increasingly large number of gyroperiods. As a consequence, direct methods remain practically limited to high-energy

particles or to localized regions [8]. Diffusion models therefore continue to serve as the primary tool for studying CR transport on Galactic scales, providing a practical balance between physical fidelity and computational feasibility, while direct numerical methods are used to validate their applicability and explore regimes where the diffusion approximation fails.

Over time, diffusion codes have grown substantially more sophisticated: they now incorporate detailed three-dimensional gas maps, modern nuclear-interaction models, realistic interstellar radiation fields, and dedicated synchrotron modules. This progress has improved the realism of simulations and improved their agreement with observations. Nevertheless, many traditional models still employ simplified, often isotropic diffusion prescriptions, assuming that the diffusion coefficient is independent of the magnetic-field orientation or adopting only simple spatial variations. At the same time, reconstructions of the large-scale Galactic magnetic field—from WMAP and Planck data, Faraday-rotation measures, and polarized synchrotron maps—indicate that the regular field component can be comparable in strength to the turbulent one (see, e.g., [9, 10]). Under such conditions, significantly different transport rates parallel and perpendicular to the magnetic field are phys-

ically expected. Numerical and theoretical studies confirm that anisotropic diffusion—manifested in the distinction between D_{\parallel} and D_{\perp} —can substantially modify CR propagation, residence times, densities, and spectra throughout the Galaxy. Anisotropic and spatially varying diffusion coefficients have been extensively investigated in works based on direct test-particle integration in turbulent fields ([11, 12], and, for extremely small ratios of gyroradius to correlation length, R_g/L_{cor} , [13]), as well as in the framework of nonlinear transport theory [14]. These studies show that the ratio D_{\parallel}/D_{\perp} can reach values of order 10^3 , while the magnetic-field structure itself produces substantial spatial inhomogeneity in the diffusion tensor. Consequently, several modified diffusion frameworks—including implementations within DRAGON—have introduced distinct parallel and perpendicular diffusion coefficients, although simplified magnetic-field geometries (e.g., axisymmetric prescriptions) are still commonly employed.

We argue that a fully anisotropic, tensorial diffusion framework—consistent with a realistic three-dimensional model of the Galactic magnetic field, including both regular and turbulent components—is essential for a proper interpretation of modern experimental data, including direct measurements of CR fluxes and diffuse γ -ray and

radio emission. This requirement is relevant because diffusion anisotropy can modify local CR spectra and the spatial distribution of emission, thereby impacting conclusions regarding acceleration mechanisms, source properties, and the structure of the interstellar medium. In most existing diffusion codes, the diffusion tensor is implemented in a simplified form. Typically, either only the flux term, $j = -D\nabla\psi$, is approximated, or parallel and perpendicular components, D_{\parallel} and D_{\perp} , are introduced under assumptions of simple magnetic-field geometry. Such treatments neglect the spatial dependence of the tensor components themselves, as well as derivative contributions that appear in the transport operator $\nabla \cdot (D\nabla\psi)$. In realistic three-dimensional magnetic-field configurations—representative of the actual Galactic structure or its local environments—a global description of diffusion using only two coefficients, D_{\parallel} and D_{\perp} , becomes insufficient. Although one can always define locally parallel and perpendicular components in an orthonormal basis aligned with the magnetic field, spatial variations of the regular field (spiral, toroidal, and vertical components) and of the turbulence amplitude lead to significant changes in the local orientation of \hat{B} and in the relative importance of D_{\parallel} and D_{\perp} . As a result, the diffusion tensor in any fixed global coordinate system becomes

highly inhomogeneous and anisotropic, with its components reflecting both the large-scale magnetic-field structure and the local turbulence spectrum and correlation length. A realistic diffusion model must therefore determine $D(\mathbf{r})$ not merely as a free parameter tuned to observations but as a quantity calibrated against direct numerical calculations of diffusion coefficients in a prescribed turbulent field. This approach ensures consistency between macroscopic diffusion models and microscopic test-particle trajectory integrations, linking first-principles estimates of diffusion coefficients with the computational efficiency of large-scale transport simulations.

Despite substantial progress in developing three-dimensional diffusion models and improving reconstructions of the Galactic magnetic field, the extent to which transport anisotropy affects observed CR spectra remains an open question. Cosmic-ray electrons are particularly sensitive to transport details because their lifetimes are dominated by strong radiative losses and decrease rapidly with energy. In this regime, both the local spectrum and the spatial distribution of electrons serve as direct diagnostics of how realistically a model captures particle transport in a three-dimensional, intrinsically anisotropic Galactic environment.

Modern measurements by DAMPE [15], CALET [16], Fermi-LAT [17], H.E.S.S. [18]

and AMS-02 [19] indicate that the electron spectrum follows a power law with index $\gamma \approx 3$ up to several hundred GeV. At energies $E \gtrsim 1$ TeV, the spectrum exhibits pronounced softening [18], corresponding to an effective index $\gamma \approx 4$. The spectral break near 1 TeV is usually attributed to a combination of effects: the limited lifetime of high-energy electrons, details of the acceleration processes in sources, and the decreasing number of nearby young sources at $E \gtrsim 1$ TeV, consistent with the shrinking lepton propagation horizon [20]. Despite notable progress, no single model currently reproduces the electron spectrum across the full energy range without considerable parameter tuning. It is generally assumed that electron acceleration proceeds via diffusive shock acceleration (DSA), producing an initial power-law spectrum with index Γ . During propagation, electrons lose energy predominantly through inverse Compton scattering and synchrotron radiation; ionization losses become negligible above a few tens of GeV. Depending on the relative magnitudes of the characteristic diffusion and loss times, three regimes may occur:

Loss-dominated regime: particles lose energy more rapidly than they diffuse, resulting in a spectral steepening by unity.

Diffusion-dominated regime: particles escape the region before losing significant en-

energy; losses do not modify the spectrum.

Mixed regime: diffusion and loss times are comparable; the spectral steepening assumes an intermediate value $\xi \in [0, 1]$.

Estimates of the diffusion coefficient inferred from secondary-to-primary nuclei ratios [21, 22], together with direct numerical calculations of the diffusion tensor [13], yield characteristic values $D \sim 10^{28} - 10^{30} \text{ cm}^2 \text{ s}^{-1}$ for energies ranging from tens of GeV to tens of TeV. These values correspond to a mixed regime transitioning into a loss-dominated regime, with the transition energy depending on the specific diffusion model. Additional spectral modifications arise from the energy dependence of diffusion, $D \propto E^\delta$, where $\delta \sim 1/3 - 1/2$ corresponds to the turbulence spectrum of the interstellar magnetic field (Kolmogorov and Kraichnan limits).

The anisotropy of the Galactic magnetic field is one of the key factors determining the transport of relativistic electrons. The regular component—characterized by a predominantly spiral structure in the disk—sets the principal direction of diffusion, whereas the turbulent component, shaped by the inhomogeneous distribution of sources and irregularities of the interstellar medium, controls the scattering rates and the turbulence spectrum. Under these conditions, diffusion becomes strongly anisotropic: the parallel coefficient D_{\parallel} often exceeds the perpendicular

coefficient D_{\perp} by several orders of magnitude. Consequently, the local electron spectrum may appear softened or hardened depending on the magnetic-field configuration, source gradients, and diffusion-tensor geometry (see, e.g., [23, 24]), and can be expressed as $E^{-(\Gamma+\delta+\xi)}$.

This paper is organized as follows. Section II describes the anisotropic diffusion model with energy losses employed in this work, along with the main features of our discretization of the diffusion equation. The construction of the diffusion tensor is discussed in detail in Sec. III. Section IV presents the software module responsible for computing energy losses in the anisotropic diffusion framework. In Sec. V, we compare different scenarios for describing the electron spectrum and its spatial distribution under various levels of approximation to the diffusion equation. We conclude with a discussion of our results in Sec. VI.

II. DISCRETIZATION OF THE ANISOTROPIC DIFFUSION OPERATOR WITH ENERGY LOSSES

The propagation of relativistic electrons and positrons in the interstellar medium is

governed by the transport equation:

$$\begin{aligned} \frac{\partial \psi(\mathbf{x}, E)}{\partial t} &= \nabla_i (D_{ij}(\mathbf{x}, E) \nabla_j \psi(\mathbf{x}, E)) \\ &\quad - \frac{\partial}{\partial E} [\alpha(\mathbf{x}, E) \psi(\mathbf{x}, E)] + Q(\mathbf{x}, E), \end{aligned} \quad (1)$$

where $\psi(\mathbf{x}, E)$ is the phase-space density, $D_{ij}(\mathbf{x}, E)$ is the anisotropic spatial diffusion tensor, $\alpha(\mathbf{x}, E)$ describes continuous energy losses, and $Q(\mathbf{x}, E)$ is the source term with a prescribed injection spectrum. Throughout this work we consider the stationary form of Eq. (1), which is appropriate for describing the Galactic background lepton population because the characteristic diffusion time τ_{diff} and the energy-loss time τ_{loss} are both short compared to the evolutionary timescales of the large-scale Galactic magnetic field and the gas distribution.

The tensor $D_{ij}(\mathbf{x}, E)$ is spatially dependent and generally non-diagonal due to the presence of an ordered Galactic magnetic field. Its energy dependence follows from the rigidity scaling of the parallel and perpendicular diffusion coefficients. A key feature of our approach is that the components of $D_{ij}(\mathbf{x}, E)$ are computed directly within a physically small local volume, where diffusion along and across the local mean magnetic field can be evaluated by integrating test-particle trajectories for a specified turbulence level. The resulting local diffusion tensor is then rotated into the global coordinate system associated with the large-scale Galactic magnetic field.

This procedure allows the use of an arbitrary (not necessarily axisymmetric) configuration of the regular magnetic field, in contrast to most diffusion models, and therefore resolve local magnetic inhomogeneities with improved accuracy.

In this section we present the finite-difference discretization used to construct a conservative and self-adjoint numerical operator on a four-dimensional grid (x, y, z, p) . Our goal is to preserve the full tensorial structure of the anisotropic diffusion operator, retain the correct transport properties along and across magnetic-field lines, and ensure numerical stability in the presence of strong radiative energy losses.

We denote the spatial grid spacings by (h_x, h_y, h_z) and employ a logarithmic momentum grid, which is a natural choice for leptonic transport where the dominant losses scale as $|\dot{p}| \propto p^2$.

Diagonal diffusion terms. For the diagonal components D_{ii} we employ a face-centered discretization that preserves the conservative structure of $\nabla \cdot (D \nabla \psi)$. The coefficient at the interface $i + \frac{1}{2}$ is approximated as

$$D_{ii}^{i+\frac{1}{2}} = \frac{1}{2} \left[D_{ii}(\mathbf{x}) + D_{ii}(\mathbf{x} + \hat{i}) \right], \quad (2)$$

leading to the discrete contribution

$$\mathcal{L}_{ii}[\psi] \approx \frac{D_{ii}^{i+1/2}}{h_i^2} \psi_{\mathbf{x}+\hat{i}} + \frac{D_{ii}^{i-1/2}}{h_i^2} \psi_{\mathbf{x}-\hat{i}} - \left(\frac{D_{ii}^{i+1/2} + D_{ii}^{i-1/2}}{h_i^2} \right) \psi_{\mathbf{x}}. \quad (3)$$

This symmetric stencil guarantees second-order accuracy for smooth D_{ii} , preserves the self-adjoint, negative-definite form of the diffusion operator, and therefore ensures numerical stability together with the physically correct damping of small-scale modes. In the limit of spatially uniform diffusion, the scheme reduces to the standard seven-point Laplacian in three dimensions.

Cross terms. In the presence of a large-scale magnetic field \mathbf{B} , particle transport becomes anisotropic

$$D_{ij} = D_{\parallel} b_i b_j + D_{\perp} (\delta_{ij} - b_i b_j), \quad (4)$$

$$b_i = B_i / |\mathbf{B}|.$$

In Cartesian coordinates this produces non-zero off-diagonal components D_{ij} for $i \neq j$, corresponding to correlated diffusion in different spatial directions.

The mixed derivative term

$$\partial_i (D_{ij} \partial_j \psi) \quad (5)$$

is discretized using a symmetric four-point corner stencil

$$\partial_i \partial_j \psi \implies \frac{\psi_{\hat{i}+\hat{j}} - \psi_{\hat{i}-\hat{j}} - \psi_{-\hat{i}+\hat{j}} + \psi_{-\hat{i}-\hat{j}}}{4h_i h_j}. \quad (6)$$

To preserve self-adjointness of the full operator, the diffusion tensor is locally symmetrized

$$D_{ij}^{\text{sym}} = \frac{1}{2} (D_{ij} + D_{ji}), \quad (7)$$

and each of the four diagonal neighbors contributes

$$\pm \frac{D_{ij}^{\text{sym}}}{4h_i h_j}. \quad (8)$$

This discretization reproduces anisotropic transport along curved magnetic-field lines, avoids spurious grid-alignment artifacts, and remains second-order accurate for smooth $D_{ij}(\mathbf{x})$.

Terms involving spatial gradients of D_{ij} .

In realistic Galactic magnetic-field and turbulence models, the diffusion tensor varies substantially across the Galaxy. The divergence operator therefore contains additional contributions

$$(\partial_i D_{ij}) \partial_j \psi, \quad (9)$$

which must be included explicitly whenever $D_{ij}(\mathbf{x})$ has strong spatial gradients.

The spatial derivative of the tensor is approximated via a centered difference

$$(\partial_i D_{ij})_c \approx \frac{D_{ij}(\mathbf{x} + \hat{i}) - D_{ij}(\mathbf{x} - \hat{i})}{2h_i}, \quad (10)$$

and the derivative of ψ analogously

$$(\partial_j \psi)_c \approx \frac{\psi_{\mathbf{x}+\hat{j}} - \psi_{\mathbf{x}-\hat{j}}}{2h_j}. \quad (11)$$

The product contributes to the $\pm \hat{j}$ neighbors with coefficients

$$\psi_{\mathbf{x} \pm \hat{j}} \longrightarrow \pm \frac{D_{ij}(\mathbf{x} + \hat{i}) - D_{ij}(\mathbf{x} - \hat{i})}{4h_i h_j}. \quad (12)$$

These terms are necessary to ensure that the full discrete operator correctly approximates $\nabla_i(D_{ij}\nabla_j\psi)$ in the presence of spatially varying anisotropic diffusion, especially where magnetic-field gradients or turbulence transitions are sharp.

Momentum-space drift from energy losses. Continuous energy losses—dominated by synchrotron radiation, inverse Compton scattering, bremsstrahlung and ionization—enter the transport equation as a convective (drift) term in momentum space. On a logarithmic momentum grid the cell spacing is

$$\Delta p_j = h_p \ln 10 E_j, \quad (13)$$

and the face-centered loss coefficients are evaluated as

$$\alpha_{j\pm\frac{1}{2}} = \frac{1}{2} [\alpha(\mathbf{x}, p_j) + \alpha(\mathbf{x}, p_{j\pm 1})]. \quad (14)$$

The corresponding upwinded discrete operator becomes

$$\mathcal{L}_p[\psi] = \frac{\alpha_{j+\frac{1}{2}}}{\Delta p_j} \psi_{j+1} - \frac{\alpha_{j-\frac{1}{2}}}{\Delta p_j} \psi_j. \quad (15)$$

Because physical losses satisfy $\alpha > 0$, the drift is always directed toward lower momenta; hence an upwind discretization is required to avoid unphysical oscillatory solutions and to maintain monotonicity of ψ . At high energies (\gtrsim few $\times 100$ GeV) this term dominates over spatial diffusion and defines the effective cooling horizon for leptons.

III. CALCULATION OF THE DIFFUSION TENSOR IN THE PRESENCE OF REGULAR MAGNETIC FIELD

In a sufficiently small physical volume—i.e., on scales comparable to the particle displacements required to reach the diffusive regime—a local coordinate system (x', y', z') can be introduced such that the z' axis is aligned with the regular magnetic field $\mathbf{B}_0 = (B_x, B_y, B_z)$. In this local field-aligned frame the diffusion tensor is diagonal:

$$\mathbf{D}' = \begin{pmatrix} D_{\perp} & 0 & 0 \\ 0 & D_{\perp} & 0 \\ 0 & 0 & D_{\parallel} \end{pmatrix}, \quad (16)$$

where D_{\parallel} and D_{\perp} denote the parallel and perpendicular diffusion coefficients obtained from test-particle simulations in a prescribed turbulent field.

To express the diffusion tensor in the global Galactic Cartesian coordinates (x, y, z) , associated with the large-scale structure of the Milky Way, we perform a rotation using the matrix \mathbf{R} :

$$\mathbf{D}^{\text{fd}} = \mathbf{R} \mathbf{D}' \mathbf{R}^T. \quad (17)$$

The orientation of the regular magnetic field \mathbf{B}_0 is parametrized by the polar and az-

imuthal angles

$$\begin{aligned}\cos \Theta &= \frac{B_z}{|\mathbf{B}_0|}, & \sin \Theta &= \frac{\sqrt{B_x^2 + B_y^2}}{|\mathbf{B}_0|}, \\ \cos \Phi &= \frac{B_x}{\sqrt{B_x^2 + B_y^2}}, & \sin \Phi &= \frac{B_y}{\sqrt{B_x^2 + B_y^2}}.\end{aligned}\tag{18}$$

The corresponding rotation matrix is

$$\mathbf{R} = \begin{pmatrix} \cos \Phi \cos \Theta & \sin \Phi & \cos \Phi \sin \Theta \\ -\sin \Phi \cos \Theta & \cos \Phi & -\sin \Phi \sin \Theta \\ -\sin \Theta & 0 & \cos \Theta \end{pmatrix}.\tag{19}$$

The regular field \mathbf{B}_0 is adopted from the Unger24 model [10], which refines standard spiral-arm based descriptions of the large-scale Galactic field. The amplitude of the turbulent component $\delta B(x, y, z)$ is modeled analytically. In this work we adopt a widely used JF12 prescription [9].

We assume isotropic turbulence with a constant correlation length $\ell_c = 50$ pc, following Ref. [13]. This approximation enables a physically consistent calculation of the parallel and perpendicular diffusion coefficients as functions of the local regular magnetic field without introducing additional model-dependent uncertainty. Although more complex scenarios are often discussed in the literature—including enhanced turbulence near supernova remnants or in the Galactic center region [25], as well as anisotropic turbulence—the present isotropic approximation is sufficient to capture the

dominant effects of anisotropic diffusion and avoids introducing poorly constrained parameters for which no comprehensive numerical benchmarks currently exist.

The parallel and perpendicular diffusion coefficients are computed using test-particle trajectory integration in the combined regular and turbulent magnetic field, following the method described in Ref. [23]. Once D_{\parallel} and D_{\perp} are determined locally in the field-aligned frame, the full diffusion tensor in Galactic coordinates is obtained by applying the rotation (17). In general, the resulting diffusion tensor is symmetric and contains up to six independent non-zero components. Its spatial variation reflects the non-uniform redistribution of cosmic rays driven by the changing magnetic-field geometry and turbulence properties throughout the Galactic volume.

IV. ENERGY LOSSES OF RELATIVISTIC ELECTRONS AND POSITRONS

To solve the stationary diffusion-loss transport equation for cosmic-ray electrons and positrons, we implement a dedicated numerical module that evaluates the total energy-loss function $\alpha(\mathbf{x}, E)$ at each spatial point and momentum node. The loss operator enters the transport equation in the stan-

standard form

$$\frac{\partial}{\partial E}[\alpha(\mathbf{x}, E) \psi(\mathbf{x}, E)], \quad (20)$$

and is discretized using an upwind finite-difference scheme (Eqs. (14) and (15)).

The total energy-loss rate is decomposed into the four dominant channels:

$$\alpha(\mathbf{x}, E) = b_{\text{syn}} + b_{\text{IC}} + b_{\text{brem}} + b_{\text{coul}}, \quad (21)$$

each evaluated locally from the magnetic field, interstellar radiation-field (ISRF) energy densities, gas density, and thermal electron density at the given Galactic position.

The magnetic field affects the transport equation exclusively through the synchrotron loss term via the local magnetic energy density $U_B = B^2/(8\pi)$. Throughout this work we employ the same large-scale Galactic magnetic-field model as used in our computation of the diffusion tensor, including the disk, toroidal-halo, and X-shaped poloidal components.

The interstellar radiation field consists of the CMB and the infrared (IR), optical, and ultraviolet (UV) components. All non-CMB components are modeled using a spatially varying energy density

$$U_{\text{ph}}(R, z) = U_0 \exp\left[-\frac{R - R_0}{R_{\text{ph}}}\right] \times \exp\left(-\frac{|z|}{z_{\text{ph}}}\right), \quad (22)$$

whereas the CMB is treated as spatially uniform. For inverse Compton (IC) losses

we adopt a performance-optimized Moderski-type approximation [26] in which each ISRF component is characterized by an effective mean photon energy.

Figure 1 shows the typical energy dependence of the individual loss terms at the Solar position, $(x, y, z) = (-8.2, 0, 0.2)$ kpc, in a Cartesian coordinate system centered on the Galactic center.

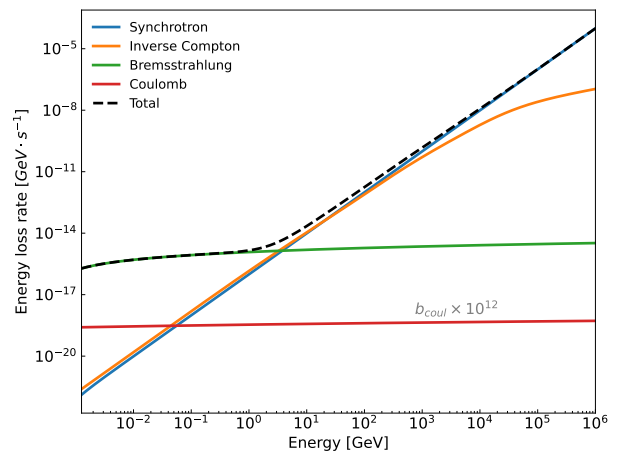


FIG. 1. Energy-loss rate as a function of lepton energy at the Solar position. The magnetic field is taken from model [10], ISRF energy densities from Ref. [27], and radiative and Coulomb loss formulae from Ref. [28].

Given the local magnetic energy density U_B , the synchrotron cooling rate is

$$b_{\text{syn}}(E) = \frac{4}{3} \sigma_T c \gamma^2 U_B, \quad (23)$$

where $\gamma = E/(m_e c^2)$. Both ordered and turbulent magnetic-field components are included.

The inverse Compton loss rate is obtained by summing the contributions from all ISRF components:

$$b_{\text{IC}}(E) = \sum_i \frac{4}{3} \sigma_{\text{TC}} \gamma^2 U_{\text{ph},i} F_{\text{KN}}(E, T_i), \quad (24)$$

where F_{KN} accounts for Klein–Nishina suppression. For the suppression factor we use the approximation

$$F_{\text{KN}}(q) = (1 + 4q)^{-3/2}, \quad q = \frac{4\gamma \varepsilon_{\text{mean}}}{m_e c^2}. \quad (25)$$

Bremsstrahlung losses depend on the local gas density n_{gas} . In the relativistic regime we employ the standard approximation

$$b_{\text{brem}}(E) \simeq 1.51 \times 10^{-16} n_{\text{gas}} \times [\ln(\gamma) + 0.36] \text{ GeV s}^{-1}, \quad (26)$$

which provides an accurate description across the relevant energy range.

Coulomb losses depend primarily on the thermal electron density n_e :

$$b_{\text{coul}}(E) \simeq 3.3 \times 10^{-29} n_e \times \left[\frac{\ln(\gamma/n_e)}{75} + 0.2 \right] \text{ GeV s}^{-1}. \quad (27)$$

This expression captures the characteristic logarithmic dependence of low-energy interactions with the ambient plasma.

At energies above several tens of GeV, synchrotron and inverse Compton losses dominate, while bremsstrahlung and Coulomb losses become negligible. Our treatment reproduces the onset of the

Klein–Nishina regime for scattering on the UV component at energies $\gtrsim 40$ GeV. The combined synchrotron and IC loss rate in our model is consistent with that used in the Unger24 framework and with the loss model of Ref. [29], but exceeds the corresponding rate adopted in GALPROP due to the larger magnetic-field strengths and radiation-field densities used here. The resulting cooling rate provides a consistent description of the local electron spectrum within the anisotropic diffusion framework.

V. RESULTS

We consider a diffusion model operating in the mixed transport regime, with a transition to the loss-dominated regime over the energy range (0.04–60) TeV. The local electron spectra are determined by the injection spectrum of the sources (a broken power law), modified by energy losses during propagation, $\alpha(\mathbf{r}, E)$, and by diffusion, $D_{\parallel, \perp} \sim E^\delta$. We assume that primary electrons are accelerated at SNR shock fronts [30]. The spatial distribution of SNRs follows the spiral-arm structure adopted in Ref. [31]. The injection index Γ , the normalization Q_0 , and the break energy in the injection spectrum E_c are treated as free model parameters. Following Ref. [32], we also include the contribution of electrons and positrons accelerated in pul-

sar wind nebulae (PWNe), assuming a broken–power–law injection spectrum with slope ~ 1.5 up to 550 GeV and ~ 2.4 at higher energies. We find that a PWNe contribution of $\epsilon_{\text{PWN}} = 9\%$ relative to the SNR component in the vicinity of the Solar System is sufficient to reproduce the data. We note, however, that larger values up to $\epsilon_{\text{PWN}} = 15\%$ have been reported, e.g., in Ref. [29], and the overall pulsar contribution to the observed spectrum remains the subject of active discussion [33]. We also model the secondary electrons and positrons produced in interactions of CR nuclei with the interstellar medium (ISM). The gas distribution is adopted from Ref. [3], and we treat CR protons as the dominant channel for secondary lepton production. The proton spectrum is computed at every grid point of the Galactic volume so as to reproduce the AMS-02 spectrum at the Solar position, in agreement with our earlier work [23]. We find that the secondary contribution remains subdominant across the entire energy range, reaching at most $\sim 4\%$ of the primary SNR electron flux at 50 GeV.

Figure 2 shows the best–fit spectrum corresponding to the optimal parameter sets $(\delta_{\text{esc}}, Q_0, E_c)$ obtained in the Monte Carlo exploration of the anisotropic model. Here we vary the parameter δ_{esc} , which accounts for the additional softening of the spectrum upon escape from the acceleration region, and as-

sume an injection index $\Gamma_0 = 2$, following Ref. [34]. Thus, the post–acceleration spectrum is expressed as $\Gamma = \Gamma_0 + \delta_{\text{esc}}$. Because of the computational cost, the minimization was performed in two stages: on a coarse grid and then on a refined grid around the lowest local minimum for the parameter ranges listed in Table I.

We perform calculations for two models. Model A includes both the spatial and energy dependence of the full diffusion tensor $\hat{D}_{ij}(\mathbf{r}, E)$ as described in Sec. III, i.e., the fully anisotropic case. Model B assumes spatially uniform diffusion coefficients with $D_{\parallel} = D_{\perp} = D_0$ and a simple power–law scaling $D(E) = D_0 E^{1/3}$, i.e., the isotropic case. The best–fit parameters are summarized in Table II. We do not display Model B in Fig. 2

TABLE I. Number of realizations N , model parameters $(\delta_{\text{esc}}, Q_0, E_c)$, and parameter ranges explored in the fitting procedure for Models A and B.

N	δ_{esc}	Q_0 ($\text{TeV}^{-1} \text{ s}^{-1} \text{ kpc}^{-3}$)	E_c (TeV)
Model A			
3375	0.100–0.250	5×10^{-23} – 1×10^{-21}	0.8–4.0
343	0.169–0.171	3×10^{-22} – 4×10^{-22}	1.2–1.4
Model B			
3375	0.200–0.400	5×10^{-22} – 1×10^{-20}	0.8–4.0
343	0.342–0.345	8×10^{-21} – 9×10^{-21}	1.1–1.3

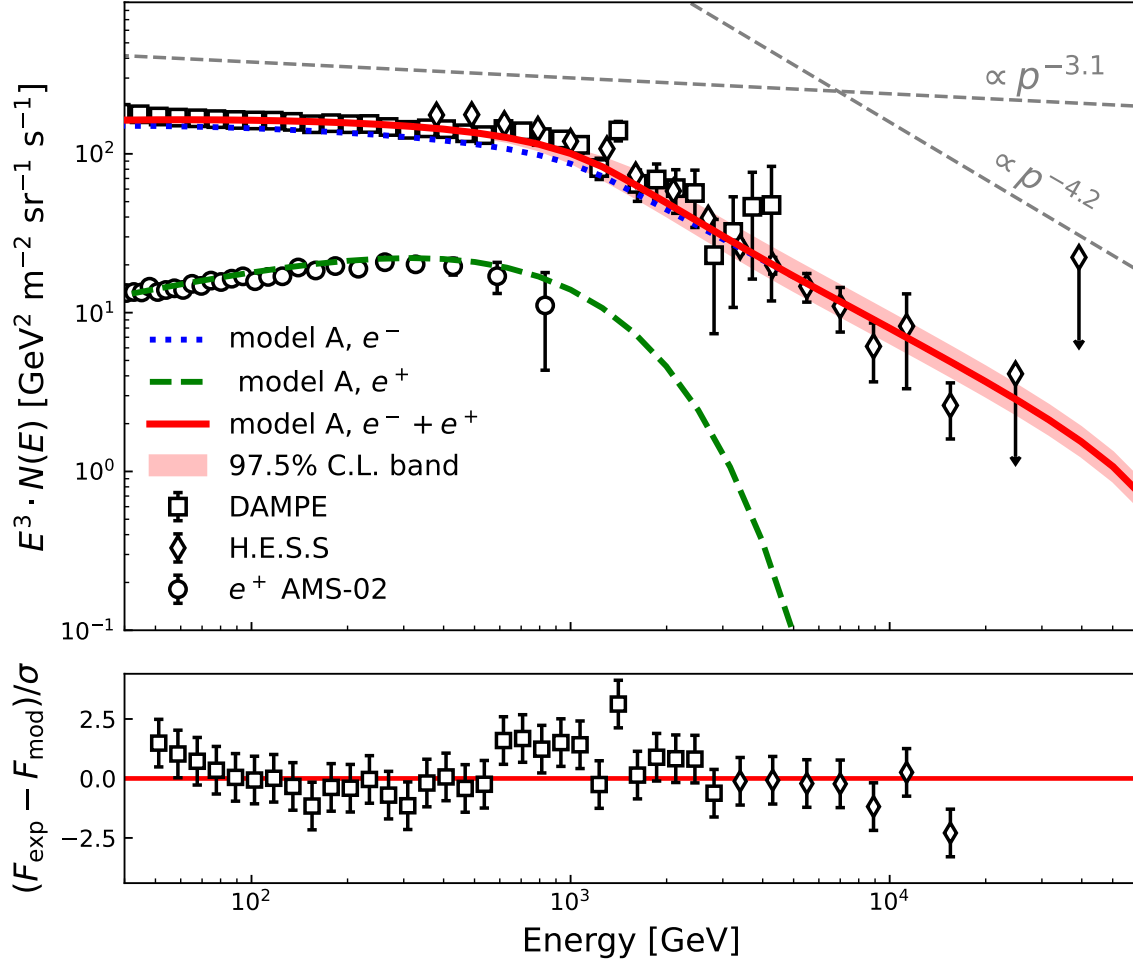


FIG. 2. Fit to the combined $e^- + e^+$ spectrum using DAMPE [15], H.E.S.S.[18] data for the total lepton flux and AMS-02 [19] data for the positron fraction over the energy interval (0.04–60) TeV. The upper panel shows the best-fit spectrum, and the lower panel shows the residuals normalized to σ . DAMPE data points overlapping with the H.E.S.S. energy range, as well as H.E.S.S. points with only upper energy bounds, were excluded from the fit.

because its spectrum remains within the uncertainty band of Model A and reproduces the local spectral shape comparably well.

We find that both models can reproduce the observed local $e^- + e^+$ spectrum; however, the isotropic Model B requires a significantly larger injection index than the anisotropic

Model A, in which the spectrum naturally softens due to the enhanced contribution of sources located along the direction of the regular Galactic magnetic field. We find that the observed lepton spectrum can be reproduced by the background SNR distribution for the primary electrons, together with the

secondary component and a modest contribution from nearby sources, which contributes noticeably only in the TeV range. This is consistent with the high degree of spectral uniformity observed up to TeV energies.

For the best-fit parameters of Model A ($\Gamma = 2.169$, $Q_0 = 3.169 \times 10^{-22}$, $E_c = 1.333$), Fig. 3 shows the $e^- + e^+$ density in two Cartesian slices of the Galaxy.

The left panel corresponds to 15 GeV, where diffusion and energy losses contribute comparably to the spectral shape. The right panel corresponds to 400 GeV, where losses dominate over diffusion, strongly limiting the distance from which CR leptons can reach the observer. The upper panels show a slice at $z = 0.2$ kpc through the Solar position, and the lower panels show a slice at $y = 0.0$ kpc. The Solar position is indicated by a star.

The ellipses indicated by gray dashed lines mark the approximate lepton propagation horizon in the anisotropic case (Model A). Following the formalism of Ref. [29] and Ref. [35] for the spatial dependence of the

diffusion-tensor components, we compute the horizon as the characteristic distance from which leptons of a given energy can reach the observer along and perpendicular to the magnetic field, rather than assuming equal diffusion radii as in isotropic models. This yields

$$\lambda_i^2(E, E_s) = 4 \int_E^{E_s} \frac{\langle D_i^{\text{fld}}(\mathbf{x}, E') \rangle}{\alpha(\mathbf{x}, E')} dE', \quad (28)$$

where $\langle D_i^{\text{fld}}(\mathbf{x}, E') \rangle$ denotes the i th component of the diffusion tensor in the local magnetic-field frame, given by Eq. 17. The true propagation region is not strictly ellipsoidal but has a more complex geometry, elongated along the regular field lines and reflecting the spatial dependence of both the diffusion tensor and the loss function, qualitatively consistent with Fig. 3.

For 15 GeV, we obtain $\lambda_{a_1, a_2, a_3} = \{9.1, 4.4, 3.8\}$ kpc, decreasing to $\{1.3, 0.6, 0.5\}$ kpc at 400 GeV, where λ_{a_1, a_2, a_3} denote the principal semi-axes of the effective propagation ellipsoid. Figure 4 shows a comparison of the propagated fluxes in Models A and B along the x and z directions for four positions in the Galaxy, marked as a, b, c, d in Fig. 3.

Both models reproduce the local lepton density near the Solar position, but at 15 GeV they show significant differences along the x direction, particularly in the inter-arm regions and near the Galactic edges. Model A yields a narrower and asymmet-

TABLE II. Best-fit values of the parameters (δ_{esc} , Q_0 , E_c) and the χ^2 values of the fits.

Model	δ_{esc}	Q_0 ($\text{TeV}^{-1} \text{ s}^{-1} \text{ kpc}^{-3}$)	E_c (TeV)	χ^2 (ndf = 37)
A	0.169	3.169×10^{-22}	1.333	27.18
B	0.344	8.833×10^{-21}	1.267	31.32

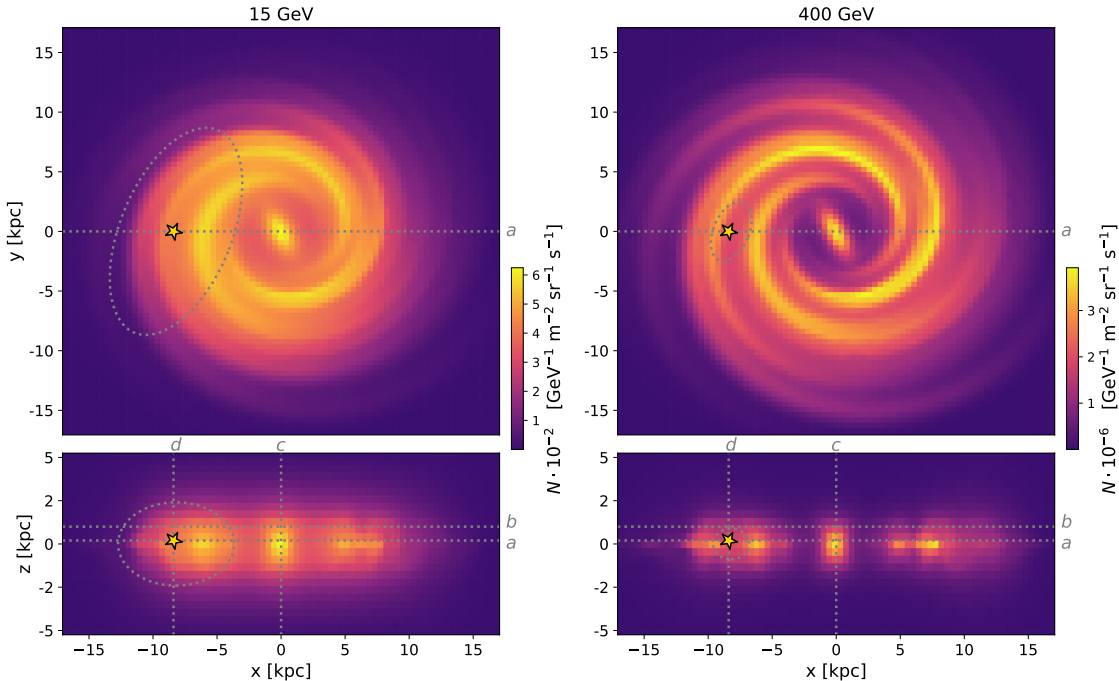


FIG. 3. Spatial distribution of CR leptons in Model A (anisotropic diffusion) at 15 GeV (left) and 400 GeV (right). The model parameters correspond to the best fit in Table II. The Solar position is marked with a star at $(x, y, z) = (-8.2, 0.0, 0.2)$ kpc. The ellipses indicated by gray dashed lines represent the approximate shape of the lepton propagation horizon.

ric profile, reflecting the preferential transport of CR leptons along the regular magnetic-field direction, which facilitates CR leakage. The vertical (z) profiles in the anisotropic Model A are broader than in Model B due to enhanced leakage into the Galactic halo. At 400 GeV, the anisotropic and isotropic profiles become more similar, reflecting the reduced lepton horizon and the increasing dominance of the source distribution over transport effects. Noticeable differences remain only in regions far from the sources—at large Galactocentric radii and

above the disk—where anisotropic leakage continues to play a significant role.

VI. CONCLUSION

We have presented a method for constructing a fully spatially dependent anisotropic diffusion tensor based on direct numerical integration of charged-particle trajectories in a realistic Galactic magnetic field, and for incorporating this tensor into a finite-difference transport scheme that explicitly accounts for spatial gradients of

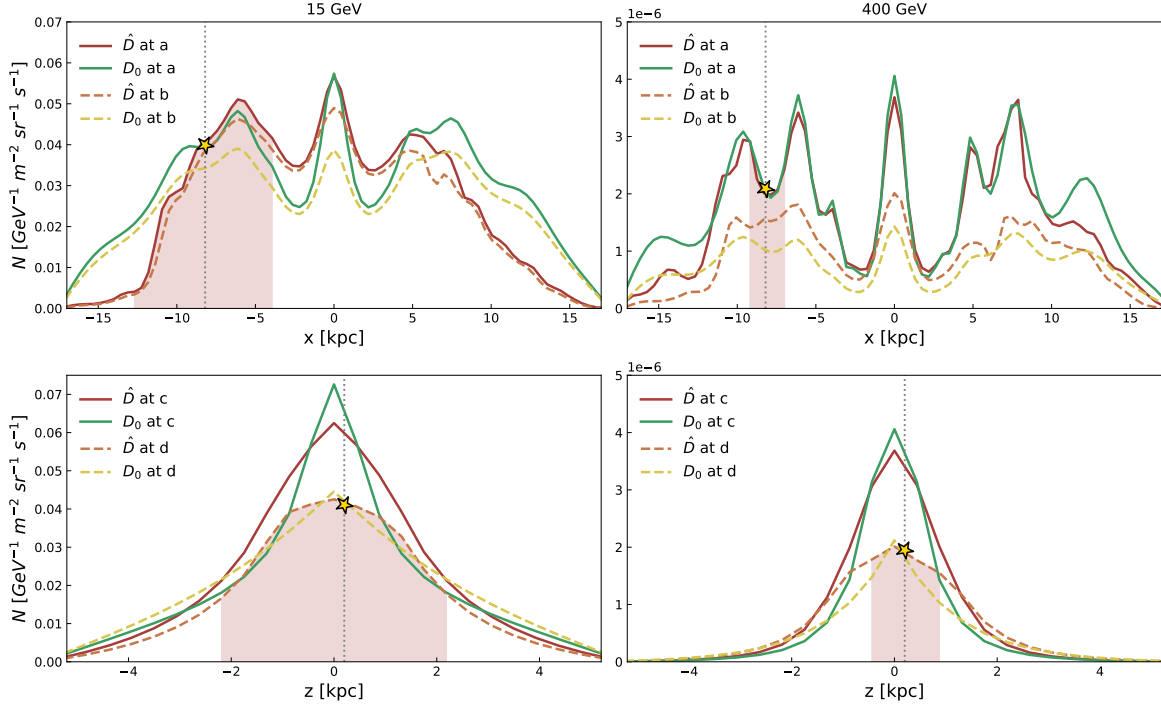


FIG. 4. Comparison of $e^- + e^+$ distributions in Model A (anisotropic diffusion \hat{D}) and Model B (isotropic diffusion D_0) at 15 GeV (left) and 400 GeV (right). The profiles are shown along x at locations a ($y = 0.0, z = 0.2$) and b ($y = 0.0, z = 1.0$), and along z at locations c ($x = 0.0, y = 0.0$) and d ($x = -8.2, y = 0.0$) kpc. The shaded regions indicate the characteristic lepton horizon. The Solar position is marked with a star at $(x, y, z) = (-8.2, 0.0, 0.2)$ kpc.

its components. This approach provides a self-consistent framework for modeling cosmic-ray propagation in which spatial variations of the diffusion tensor—arising from the local magnetic-field strength and orientation—affect the resulting lepton distribution.

We have shown that the observed local spectrum of cosmic-ray electrons and positrons can be reproduced within a diffusion framework operating in the early stages of the transition to the loss-dominated

regime, at energies of several tens of GeV. In this regime, the spectrum can be matched without introducing multiple breaks either in the injection spectrum or in the energy dependence of the diffusion tensor. Under mixed-transport conditions, anisotropic diffusion produces a narrower spatial profile of cosmic-ray leptons due to preferential propagation along magnetic-field lines. In the loss-dominated regime, by contrast, the spatial distribution of sources becomes the primary factor shaping the observed lepton distribu-

tion, as energy losses restrict the distance from which cosmic-ray leptons can reach the observer.

We also find that allowing for spatially varying anisotropic diffusion reduces the required injection index compared to isotropic models. This behavior arises because anisotropic transport enables leptons to propagate over larger effective distances along the regular magnetic field before losing their energy—corresponding to an increased effective propagation horizon. Consequently, our results suggest that models assuming intrinsically hard electron injection spectra may not be required: the observed local spectrum can be explained by the diffuse Galactic source population, provided that energy losses during transport are treated consistently.

Finally, we find that the observed lepton spectrum can be reproduced within the anisotropic diffusion framework without in-

voking dominant contributions from nearby individual sources. If such sources contribute at TeV energies, their effect on the local spectrum must remain subdominant. This conclusion is consistent with the absence of strong anisotropy in the high-energy cosmic-ray lepton flux.

ACKNOWLEDGMENTS

The research was supported by RSF (project No.25-22-00246).

DATA AVAILABILITY

The experimental data used in this work are publicly available from the sources cited in Refs. [15], [18] and [19]. For a more detailed description of the mathematical framework employed in this study, see Refs. [23], [24] and [36]. The code developed for data processing and analysis is available from the corresponding author upon reasonable request.

[1] G. M. Webb, J. R. Jokipii, and G. E. Morfill, Green’s formula and variational principles for cosmic-ray transport with application to rotating and shearing flows, *Astrophys. J.* 424, 158 (1994).

[2] M. Hanasz, G. M. Webb, J. R. Jokipii, and G. E. Morfill, Simulations of cosmic ray

propagation, *Living Rev. Comput. Astrophys.* 7, 2 (2021).

[3] A. W. Strong and I. V. Moskalenko, Propagation of cosmic-ray nucleons in the galaxy, *Astrophys. J.* 509, 212 (1998).

[4] C. Evoli, D. Gaggero, A. Vittino, G. Di Bernardo, M. Di Mauro, A. Ligorini, P. Ul-

- lio, and D. Grasso, Cosmic-ray propagation with DRAGON2: I. numerical solver and astrophysical ingredients, *JCAP* 02, 015 (2017).
- [5] R. A. Batista, A. Dundovic, M. Erdmann, K.-H. Kampert, D. Kuempel, G. Müller, G. Sigl, A. van Vliet, D. Walz, and T. Winchen, CRPropa 3 — a public astrophysical simulation framework for propagating extraterrestrial ultra-high energy particles, *JCAP* 05, 038 (2016).
- [6] G. Giacinti, M. Kachelriess, and D. V. Semikoz, Filamentary diffusion of cosmic rays on small scales, *Phys. Rev. Lett.* 108, 261101 (2012).
- [7] A. Y. Prosekin, S. R. Kelner, and F. A. Aharonian, On transition of propagation of relativistic particles from the ballistic to the diffusion regime, *Phys. Rev. D* 92, 083003 (2015).
- [8] G. Giacinti, M. Kachelrieß, and D. V. Semikoz, Escape model for Galactic cosmic rays and an early extragalactic transition, *Phys. Rev. D* 91, 083009 (2015).
- [9] R. Jansson and G. R. Farrar, A new model of the Galactic magnetic field, *Astrophys. J.* 757, 14 (2012).
- [10] M. Unger and G. R. Farrar, The coherent magnetic field of the Milky Way, *Astrophys. J.* 970, 95 (2024).
- [11] R. Casse, M. Lemoine, and G. Pelletier, Transport of cosmic rays in chaotic magnetic fields, *Phys. Rev. D* 65, 023002 (2002).
- [12] A. Dundovic, O. Pezzi, P. Blasi, C. Evoli, and W. H. Matthaeus, Novel aspects of cosmic ray diffusion in synthetic magnetic turbulence, *Phys. Rev. D* 102, 103016 (2020).
- [13] M. Kuhlen, V. H. M. Phan, and P. Mertsch, Diffusion of relativistic charged particles and field lines in isotropic turbulence: I. Numerical simulations, *Astrophys. J.* 992, 10 (2025).
- [14] M. Shalchi, Nonlinear cosmic ray diffusion theories, (Springer, Berlin, 2009).
- [15] DAMPE Collaboration, Direct detection of a break in the teraelectronvolt cosmic-ray spectrum of electrons and positrons, *Nature* 552, 63–66 (2017).
- [16] O. Adriani et al. (the CALET Collaboration), Energy spectrum of cosmic-ray electron and positron from 10 GeV to 3 TeV observed with the calorimetric electron telescope on the International Space Station, *Phys. Rev. Lett.* 119, 181101 (2017).
- [17] S. Abdollahi, M. Ackermann, M. Ajello, et al. (the Fermi-LAT Collaboration), Cosmic-ray electron-positron spectrum from 7 GeV to 2 TeV with the Fermi Large Area Telescope, *Phys. Rev. D* 95, 082007 (2017).
- [18] F. Aharonian, F. Ait Benkhali, J. Aschersleben, et al. (the H.E.S.S. Collaboration),

- High-statistics measurement of the cosmic-ray electron spectrum with H.E.S.S., *Phys. Rev. Lett.* 133, 221001 (2024).
- [19] M. Aguilar, L. Ali Cavazonza, G. Ambrosi, et al. (the AMS-02 Collaboration), Precision measurement of the electron flux in primary cosmic rays from 0.5 GeV to 1 TeV with AMS-02, *Phys. Rev. Lett.* 113, 221102 (2014).
- [20] S. Thoudam, Origin of the break in the cosmic-ray electron plus positron spectrum at 1 TeV, *Astron. Astrophys.* 690, A351 (2024).
- [21] P. de la Torre Luque, M. N. Mazziotta, F. Loparco, F. Gargano, and D. Serini, Markov chain Monte Carlo analyses of the flux ratios of B, Be and Li with the DRAGON2 code, *JCAP* 07, 010 (2021).
- [22] J.-S. Niu and T. Li, Galactic cosmic-ray model in the light of AMS-02 nuclei data, *Phys. Rev. D* 97, 023015 (2018).
- [23] V. D. Borisov, V. O. Yurovsky, and A. I. Peryatinskaya, Spatial dependence of the break in the energy spectrum of cosmic rays in the new anisotropic diffusion approach, *Phys. Rev. D* 112, 023010 (2025).
- [24] V. D. Borisov, V. O. Yurovsky, and I. A. Kudryashov, Modulation of the galactic cosmic ray spectrum in an anisotropic diffusion approach, *Bull. Russ. Acad. Sci. Phys.* 89, 1019–1023 (2025).
- [25] O. Iffrig and P. Hennebelle, Structure distribution and turbulence in self-consistently supernova-driven ISM of multiphase magnetized galactic discs, *Astron. Astrophys.* 604, A70 (2017).
- [26] R. Moderski, M. Sikora, P. S. Coppi, and F. Aharonian, Klein–Nishina effects in the spectra of non-thermal sources immersed in external radiation fields, *Astrophys. J.* 630, 130–136 (2005).
- [27] T. Delahaye, J. Lavalle, R. Lineros, F. Donato, and N. Fornengo, Galactic electrons and positrons at the Earth: new estimate of the primary and secondary fluxes, *Astron. Astrophys.* 524, A51 (2010).
- [28] G. R. Blumenthal and R. J. Gould, Bremsstrahlung, synchrotron radiation, and Compton scattering of high-energy electrons traversing dilute gases, *Rev. Mod. Phys.* 42, 237–270 (1970).
- [29] C. Evoli, P. Blasi, E. Amato, and R. Aloisio, The signature of energy losses on the cosmic ray electron spectrum, *Phys. Rev. Lett.* 125, 051101 (2020).
- [30] V. N. Zirakashvili and F. Aharonian, Analytical solutions for energy spectra of electrons accelerated by nonrelativistic shockwaves in shell type supernova remnants, *Astron. Astrophys.* 465, 695–702 (2007).
- [31] P. Blasi and E. Amato, Diffusive propagation of cosmic rays from supernova rem-

- nants in the Galaxy. I: spectrum and chemical composition, *JCAP* 01, 010 (2012).
- [32] E. Amato and P. Blasi, Cosmic ray transport in the Galaxy: a review, *Adv.Space Res.* 62, 2731–2749 (2018).
- [33] S. Manconi, M. Di Mauro, and F. Donato, Contribution of pulsars to cosmic-ray positrons in light of recent observation of inverse-Compton halos, *Phys. Rev. D* 102, 023015 (2020).
- [34] M. Wolff and R. C. Tautz, Cosmic-ray acceleration at collisionless astrophysical shocks using Monte-Carlo simulations, *Astron. Astrophys.* 580, A58 (2015).
- [35] P. C. Bressloff and S. D. Lawley, Moment equations for a piecewise deterministic PDE, *J. Phys. A: Math. Theor.* 48, 105001 (2015).
- [36] V. D. Borisov and I. A. Kudryahshov, Four-Dimensional Anisotropic Diffusion of Cosmic Rays in Realistic Galactic Magnetic Fields, *PoS(ICRC2025)* 016 (2025).